Original article
DOI: https://doi.org/10.18721/JPM.15309

NUMERICAL SIMULATION OF TURBULENT AIRFLOW AND HEAT TRANSFER AROUND A SEATED THERMAL MANIKIN IN THE ROOM WITH MIXING VENTILATION

M. A. Zasimova, A. A. Marinova, N. G. Ivanov✉, A. D. Podmarkova

Peter the Great St. Petersburg Polytechnic University, St. Petersburg, Russia

✉ ivanov_ng@spbstu.ru

Abstract. The numerical simulation of turbulent flow and heat transfer, when air moves around a thermal manikin sitting in a model room with mixing ventilation, has been carried out. The calculations were performed on the basis of the RANS approach using the standard k-ε turbulence model. The buoyancy effects were described in the Boussinesq approximation. The obtained calculated data were close to the experimental ones, although there were local differences in the temperature distribution near the surface of the room walls. The impossibility of correct determination of the integral heat removal from the surface of the body without taking into account the radiation heat transfer was established. Along with studies in the ventilation regime with predominant forced convection, corresponding to the experiment, the characteristics of the flow and heat transfer in the free convection regime were analyzed, where the flow structure being caused by an intensive thermal plume forming above the manikin, and the temperature field being stratified in height.

Keywords: ventilation, thermal mannequin, turbulent airflow, heat transfer, natural and forced convection

Funding: The research work was supported by a grant from the President of the Russian Federation (No. MK-1762.2022.1.1).

Citation: Zasimova M. A., Marinova A. A., Ivanov N. G., Podmarkova A. D., Numerical simulation of turbulent airflow and heat transfer around a seated thermal manikin in the room with mixing ventilation, St. Petersburg Polytechnical State University Journal. Physics and Mathematics. 15 (3) (2022) 111–131. DOI: https://doi.org/10.18721/JPM.15309

Научная статья
УДК 532.517
DOI: https://doi.org/10.18721/JPM.15309

ЧИСЛЕННОЕ МОДЕЛИРОВАНИЕ ВОЗДУШНЫХ ПОТОКОВ ПРИ ОБТЕКАНИИ СИДЯЩЕГО ТЕПЛОВОГО МАНЕКЕНА В ПОМЕЩЕНИИ С ПЕРЕМЕШИВАЮЩЕЙ ВЕНТИЛЯЦИЕЙ

М. А. Засимова, А. А. Маринова, Н. Г. Иванов✉, *А. Д. Подмаркова*

Санкт-Петербургский политехнический университет Петра Великого,

Санкт-Петербург, Россия

✉ ivanov_ng@spbstu.ru

Аннотация. Выполнено численное моделирование турбулентного течения и теплообмена при обтекании воздушным потоком сидящего теплового манекена, размещенного в модельном помещении с перемешивающей вентиляцией. Расчеты проведены на основе RANS-подхода с использованием стандартной k-ε модели турбулентности. Эффекты плавучести описаны в приближении Буссинеска. Полученные расчетные данные близки к экспериментальным, хотя имеются локальные отличия по распределению температуры вблизи поверхности стенок помещения. Установлено, что без учета лучистого теплообмена невозможно правильно определить интегральный теплосъем с поверхности тела. Наряду с исследованиями режима вентиляции с преобладанием вынужденной конвекции, соответствующим эксперименту, были изучены характеристики течения и теплообмена в свободноконвективном режиме, где структура течения определяется интенсивным тепловым факелом, формирующимся над манекеном, а поле температуры стратифицировано по высоте.

Ключевые слова: вентиляция, тепловой манекен, турбулентное течение, теплообмен, естественная и вынужденная конвекция

Финансирование: Работа выполнена при финансовой поддержке гранта президента Российской Федерации МК1762.2022.1.1-.

Ссылка для цитирования: Засимова М. А., Маринова А. А., Иванов Н. Г., Подмаркова А. Д. Численное моделирование воздушных потоков при обтекании сидящего теплового манекена в помещении с перемешивающей вентиляцией // Научно-технические ведомости СПбГПУ. Физико-математические науки. 2022. Т. 15. № 3. С. 111–131. DOI: https://doi.org/10.18721/JPM.15309

Introduction

Heating, ventilation, and air conditioning systems (HVAC) are aimed at ensuring thermal comfort for humans in residential structures, providing environments with controlled parameters [1, 2]. In real-life conditions, rooms are almost always occupied by people, as well as blocked by furniture or other interior objects. Computations of ventilation systems are often performed for empty rooms free of obstructions [3, 4] in order to minimize geometric uncertainties. The temperature field of a person or a group of people in the room plays the major role in assessments of thermal comfort and air quality. The thermal characteristics, as well as the general structure of the flow can vary substantially in this case. Experimental studies typically use models reproducing the human body parameters to some extent, rather than living people (whose individual characteristics are nearly impossible to reproduce).

The model of the human body can be greatly simplified; for example, lamps with heat emission corresponding to the human body were used in [5], experimentally studying the air distribution

in the room for various ventilation scenarios. However, most studies describe human-like thermal manikins (one or several) with controlled parameters, including thermal conditions on the body surface [6]. Accordingly, virtual thermal manikins that fully or partially reproduce these parameters are used for numerical simulations. One or more realistic thermal manikins were used in computations of air distribution and estimation of thermal comfort parameters in [7–9].

However, uncertainties associated with setting a large number of a priori unknown parameters appear even in applied ventilation problems formulated and solved with controlled thermal manikins; these parameters include the number of people in the room, all kinds of movements they make, the exact location of a person in space in the operating conditions, the geometric configuration (exact shape) of the body, the thermal insulation properties of clothing, etc. If all of these parameters are based on some approximate estimates, it is virtually impossible to solve the problem fully accounting for all of the given conditions, so the influence of the parameters complicating the problem is generally considered separately.

One of the parameters examined in a number of studies is the influence of the thermal manikin's shape on the characteristics of flow and heat transfer. Clearly, the shape of a physical or virtual thermal manikin can be greatly simplified. For example, simplified geometric shapes of the manikin can be used to account for obstructions in the room [10, 11]. However, it is established in [12–14], the shape of the manikin can significantly affect the local characteristics of the flow near the manikin. Four manikin shapes were considered in the experimental study in [12]: one approximating the human shape and three simplified shapes (a cylinder, a parallelepiped and a combination of these figures). Airflow computations were carried out in [13] near six manikin shapes with different details. Numerical simulation was performed in [14] for the problem with three manikin shapes (the one approximating the shape of the human body, as well as partially and completely simplified shapes composed of parallelepipeds). Studies indicate that the shape of the manikin close to the human body should be used to predict local characteristics.

Computations in unsteady conditions were carried out in [15, 16] with the position of the manikin spatially varied over time. A full-scale experiment and computer simulation (Large Eddy Simulation) were carried out in [15] to study the flow evolving for a manikin moved between rooms with different concentrations of polluted air. The door between the rooms was opened during the experiment, and the manikin was moved through the doorway, but the variations in the positions of manikin's individual parts were not taken into account. The influence of the thermal manikin's movement on stratification of the temperature field was experimentally investigated in [16]. The variables were the velocity of the manikin, the movement duration, the intensity of heat generation from the surface and the air change rate (airflow per unit time).

Generally, a clothed manikin and the specific characteristics of its clothing can significantly affect the heat transfer from its surface (see, for example, [12, 17, 18]). For example, the thermal insulation characteristics of clothing, the presence of hair on the surface of the head and the design of the chair on which the manikin was seated were varied in [12]. The effect of clothing on heat transfer was considered in [17]. The main parameter in the experimental study [18] was the type of clothing; the mannequin was dressed in light summer clothes, in warm winter clothes and in a business suit.

The respiration process of a thermal manikin was considered in [19, 20]: the periodic propagation of an air jet produced during exhalation can modify the structure of the flow near the manikin and affect the characteristics of heat and mass transfer. The unsteady processes of inhalation and exhalation through the nostrils and mouth were modeled in [19] for a sitting and standing manikin under transient conditions. The air flow was also simulated inside the manikin. The RANS-approach was applied in [20] in a steady-state formulation to simulate three phases of breathing (inhalation, exhalation and the pause between them) for a standing manikin. The review [21] considers studies that performed numerical simulation of breathing in a manikin, giving the boundary conditions (periodic breathing cycles) set in the corresponding computations on the surface of the manikin's mouth. Several recent publications are aimed at solving the crucial problem of predicting the dispersion of saliva droplets released during breathing or coughing (sneezing) [22–24].

Numerous experimental and computational studies described the structure of the flow and the characteristics of heat and mass transfer in ventilated rooms occupied by people. Efforts are also underway to validate the computational techniques, generally considering rooms unoccupied rooms (see, for example, [25–27]). Computational validations require data from well-documented

experimental tests; however, such tests are scarce for rooms with thermal manikins. Experiments at the Danish Technical University (Lyngby, Denmark) were carried out in 2003 and 2007 for the conditions of displacement [28] and mixing [28–31] ventilation (the results are compiled into a database at http://www.cfdbenchmarks.com/). Data from the test with displacement ventilation were used earlier to validate numerical simulation techniques in [14, 32, 33]. Data from the test with mixing ventilation were used earlier in [34–36]. The conditions of this test are reproduced in this paper.

The goal of our study consists in numerical analysis of the structure of turbulent flow and the characteristics of heat transfer for airflow around a sitting thermal manikin in a model room.

Computations were performed for conditions close to experimental ones [30, 31], and the results of numerical simulation are compared with the experimental data. Aside from validating the computational technique, we analyzed the influence of thermal conditions on the surface of the manikin (constant temperature or constant specific heat flux). Furthermore, the role of various heat transfer mechanisms was considered as part of the parametric study.

Problem statement

Geometric model. The model of the ventilated room corresponds to the data of experimental studies [30, 31] and is a parallelepiped with the length $L = 2.44$ m (along the axis x), height $H = 2.46$ m (along the axis y) and the width $W = 1.20$ m (along the axis z). One of the side walls of the room is open (marked as Inlet in Fig. 1,*a*); air enters the room through this interface, assumed to be an inlet opening for the computational domain. Two circular exhaust opening with the same diameter equal to $d_{out} = 0.25$ m are located on the opposite side wall (marked as Outlet in Fig. 1,*a*). The outlet openings are centered relative to the axis z, the centers of the lower and upper openings are located 0.6 m away from the floor and ceiling of the room, respectively.

A seated thermal manikin (see Fig. 1) was placed in the room 0.5 m from the open boundary (0.7 m to the manikin's knees). The distances from the manikin surface to the side walls of the room are the same in the transverse direction (axis z), amounting to 0.325 m; there is a gap 0.002 m high between the floor of the room and the manikin's feet. The geometry of the manikin is taken from the database at www.cfd-benchmarks.com, with the description of the conditions and results of the experiment. The characteristic (maximum) size of the manikin is $l_m = 0.76$ m in the longitudinal direction (along the axis x), $h_m = 1.36$ m in the vertical direction (along the axis y) and $w_m = 0.55$ m in the transverse direction (along the axis z) . The surface area of the manikin is $S_m = 1.60$ m^2.

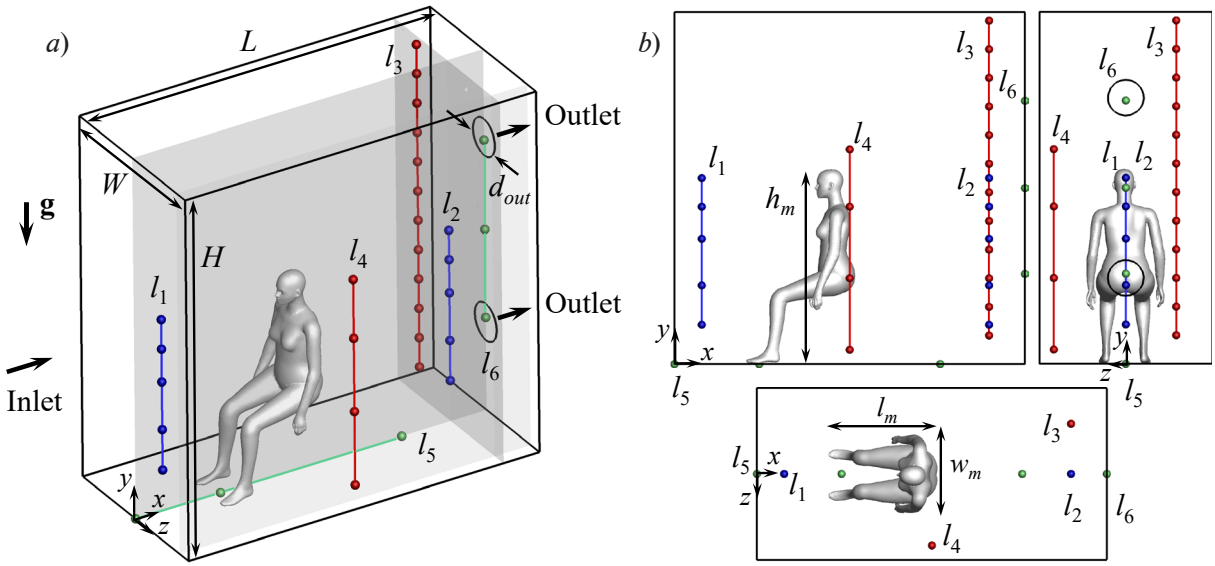

Fig. 1. Images of computational model of the room with a seated manikin in isometric projection (*a*) and in planes (*b*).
Lines l_1–l_6 show the points where the velocity (blue) and temperature (red and green) were measured (see [30, 31])

No modifications were introduced in the present study to the geometric model of the manikin provided in the database. However, as evident from the illustrations both for the experiments described in [30, 31] and for subsequent studies dedicated to numerical simulation [34, 35], the manikin was tilted by some angle relative to the vertical axis. We can therefore assume that the positions of the individual parts of the manikin in the experimental setup were different from those available in the database, although no information about this is given in either the studies or the documentation. Thus, the position of the manikin in the room is somewhat unclear, so it cannot be accounted for in the statement to the computational problem.

The positions of lines l_1–l_6 along which the measurements were carried out [30, 31] are shown in Fig. 1. The points highlighted are the ones for which experimental values are given in the database. The velocity magnitudes were measured along the lines l_1 and l_2 using a spherical thermal anemometer; the lines are located in the central section of room $z = 0$ 0.19 m and 2.19 m away from its open boundary, respectively. The temperature was measured with thermocouples along the lines l_3 and l_4 placed near the walls of the room ($x = 2.19$ m, $z = -0.35$ m and $x = 1.22$ m, $z = 0.50$, respectively), and along the lines l_5 and l_6 on the surface of the room ($y = 0$, $z = 0$ and $x = L$, $z = 0$).

Physical parameters of the environment and boundary conditions. We considered the flow of air whose properties were assumed to be constant at a temperature of 20 °C. The Prandtl number was equal to $\mathrm{Pr} = \mu C_p/\lambda = 0.7$, where μ is the dynamic viscosity equal to $1.81 \cdot 10^{-5}$ kg/(m·s); C_p is the specific heat of air at a constant pressure of 1.005 kJ/(kg·K); λ is the thermal conductivity equal to 25.9 mW/(m·K).

The computational cases with different inlet boundary conditions, thermal conditions on the manikin surface, and parameters of the physical model are given in Tables 1 and 2.

Two values of airflow rate were considered: 0.7970 m^3/s (the corresponds to the experimental value in [30, 31]) and 0.0295 m^3/s. The air in the experiment was sucked through the outlet openings, and the conditions for air inflow through the open endwall of the room ensured a uniform profile. A uniform distribution of the inlet velocity was adopted in the computations, also with two values: $V_{in} = 0.27$ and 0.01 m/s (respectively). In accordance with the experimental conditions in [30, 31], constant air temperature was maintained at the inlet boundary, equal to $T_{in} = 20.4$ °C. The Reynolds number constructed from the inlet air velocity and the width of the manikin, i.e.,

$$\mathrm{Re} = \rho w_m V_{in}/\mu,$$

where ρ is the air density equal to 1.205 kg/m^3, was Re = 366 and 9886 at $V_{in} = 0.01$ and 0.27 m/s, respectively.

With the room height used as a linear scale, the Reynolds number $\mathrm{Re}_H = \rho H V_{in}/\mu$ amounted to $\mathrm{Re}_H = 1.638$ and 44.218, respectively.

The no-slip condition was imposed at the solid boundaries of the room, the walls were assumed to be adiabatic (setting zero heat flux q_w including the conductive and the convective component). Constant pressure was imposed at the outlet boundaries.

Table 1

Boundary conditions for different computational cases

Parameter	Value for case						
	1	2	3	4	5	6	7
V_{in}, m/s	0.27				0.01		
T_w, °C	34.0	–					
q_w, W/m^2	–		139.3	80.5	139.3	66.1	139.3

Notations: V_{in} is the air velocity at the entrance to the room, T_w is the temperature at the surface of the thermal manikin, q_w is the total specific heat flux including three components (conductive, convective and radiative).

Either constant temperature T_w or constant total specific heat flux q_w including all three components (conductive, convective and radiative) were set on the surface of the manikin for different computational cases. In accordance with the experimental conditions given in [30, 31], a constant temperature equal to $T_w = 34$ °C was maintained on the manikin surface. The computational case best reproducing the experimental conditions is Case 1 in Table 1. The Grashof number, constructed from the height of the manikin,

$$\mathrm{Gr} = \rho^2 g\beta(T_w - T_{in})h_m^{\,3}/\mu^2,$$

was equal to $\mathrm{Gr} = 5.06 \cdot 10^9$ (g is the gravity acceleration, β is the thermal expansion coefficient equal to 0.0034 K^{-1}).

Notably, part of the manikin surface around the knees was thermally insulated in [30, 31]; this was not taken into account in our computations because there is no accurate data about the location of this area.

Table 2

Parameters of the physical model for computational cases

Case	1	2	3	4	5	6	7
Radiation model	+	–	+	–	+	–	+
Gravity	+						–

The computational software allowed to comprehensively analyze the contributions from various heat transfer mechanisms to integral heat removal from the manikin surface. Evidently, forced convection is predominant in Cases 1–4 and free convection in Cases 5–7; Cases 1, 3, 5, 7 accounted for the contribution from radiative heat transfer to heat removal, while radiative heat transfer was not simulated in Cases 2, 4, 6. Additional computations were carried out for low flow rate of air under zero gravity conditions (see Tables 1 and 2, Case 7): radiative heat transfer is predominant, the contribution from free convection is absent. These conditions correspond, for example, to those at the International Space Station under ventilation shutdown [37, 38].

The air in the room was assumed to be transparent for simulation of thermal radiation, the emissivity (degree of blackness) was taken equal to 0.93 for the thermal manikin and 0.83 for the solid surfaces of the room model.

Mathematical and computational model. Turbulent airflow was simulated by the RANS approach (solving the Reynolds-averaged Navier–Stokes equations); see monograph [39] for more details. The Reynolds stress tensor was calculated from the Bussinesq approximation, while the turbulent viscosity was determined by the standard k-ε turbulence model. The Enhanced Wall Treatment option was used near the solid walls. The following turbulence characteristics were set at the inlet boundary in accordance with the selected model: turbulence intensity $I = 6\%$ and the ratio of turbulent to molecular viscosity $\mu_t/\mu = 10$.

The system of governing equations for motion includes the equation for heat balance, while the buoyancy force is described in the Bussinesq approximation. The direction of the gravitational acceleration vector is marked by the arrow in Fig. 1,*a*.

Radiative energy transfer was accounted for using the surface-to-surface (S2S) model available in ANSYS Fluent. The model allows to determine the transfer of energy between differently heated solid surfaces, while the transmissivity of the body is taken equal to zero.

The computational mesh was constructed in the ICEM CFD package; the resulting mesh consisted of tetrahedral elements away from solid surfaces and prismatic layers near them. The mesh was clustered near the surface of the manikin. Five prismatic layers were set near each wall of the room without clustering, the height of the first near-wall layer was $y_p = 5$ mm; eleven prismatic layers with a clustering coefficient of 1.1 were set near the surface of the manikin, with $y_p = 1$ mm. ANSYS Fluent tools were used to convert the tetrahedral elements of the mesh to polyhedra, the total size of the transformed mesh was 590,000 cells. This mesh was used in all computations (Fig. 2,*a*).

The distribution of the dimensionless distance y^+ from the center of the first near-wall cell to the wall is shown in Fig. 2, *b*, *c*. The value of the quantity y^+ averaged 1.37 over the manikin surface, its maximum value of 3.81 was detected on the surface of the manikin's hands. The average value of y^+ on the walls perpendicular to the axes *y* and *z* was 3.34, the maximum values of y^+ lay near the outlet opening, reaching 80 locally.

The computations were performed using the ANSYS Fluent CFD package. The equations were discretized with second-order accuracy. The Coupled scheme was used to relate the fields of pressure and velocity components. The residuals in the presented computations converge in the steady-state formulation.

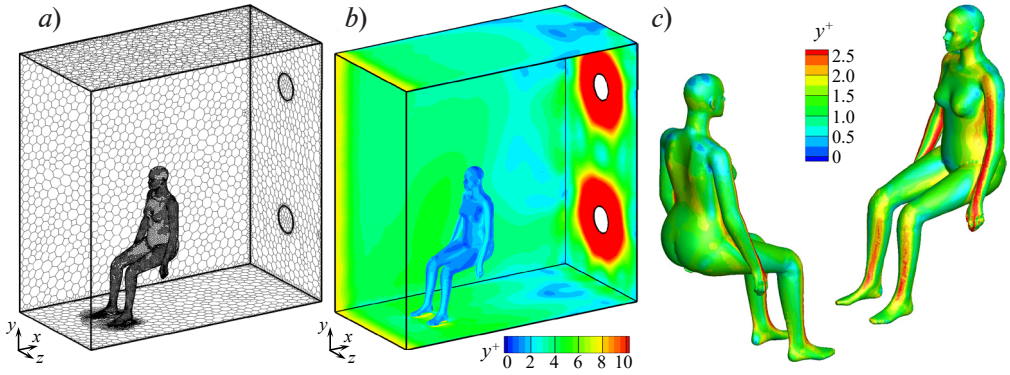

Fig. 2. Illustration of computational aspects: general view of computational mesh (*a*), distribution of quantity y^+ over the surfaces of room walls (*b*) and manikin (*c*)

Computational results

Description of the flow structure and parameters of heat transfer from the manikin surface. The general structure of the flow is illustrated based on the data obtained for Case 1, approximated to the conditions of the experiments in [30, 31]. Fig. 3 shows the streamlines colored in accordance with the velocity magnitude, as well as the velocity and temperature fields in several sections of the room. As the airflow reaches an obstacle (in this case, the manikin), it decelerates to the left and to the right around the manikin's torso; regions of accelerated flow evolve in the vicinity of the floor, where the velocities reach 0.4 m/s (see Fig. 3, *a*, *b*). An extensive separation region (with rarefied flow) appears behind the manikin. Circulation regions with slow flow are also observed near the floor and ceiling of the room, at the end wall opposite to the entrance. As the flow approaches the outlet openings, it accelerates, with the velocity level reaching 10 m/s. Notice that outflow separation is uniform: the airflow rate through the upper and lower openings is almost the same.

The temperature fields (see Fig. 3, *c*) illustrate the heating of air in the separated region behind the manikin, where the temperatures range from 34 °C at the surface to 21 °C away from the manikin. No thermal plume is observed above the manikin: it is carried away by strong incident airflow. Because the walls were assumed to be adiabatic, they are apparently heated by thermal radiation. This can be seen in Fig. 3,*c*, where the temperature field on the bottom wall is shown as an example. The mean temperatures over the surface are as follows:

21.2 °C for the ceiling,
21.6 °C for the side walls,
22.0 °C for the floor,
21.2 °C for the end wall.

As seen from Fig. 3,*c*, heating of the walls produces a slight increase in the temperature of air in their vicinity.

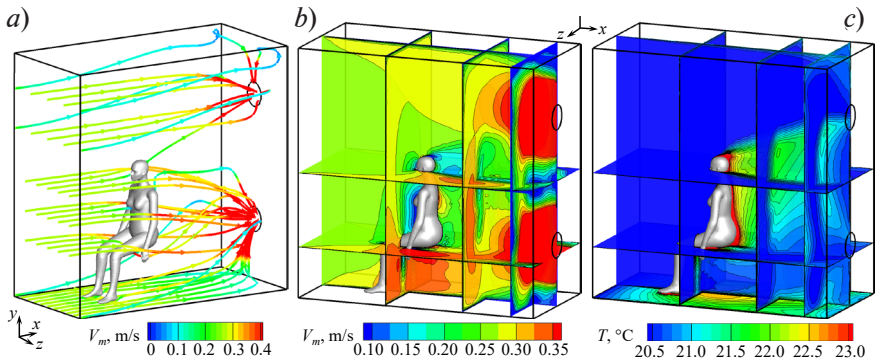

Fig. 3. Computational structure of airflow in the room, shown for Case 1 (see Table 1) by the streamlines colorized in accordance with the velocity magnitudes (*a*), fields of velocity magnitude (*b*) and temperature (*c*) in several sections of the room

Fig. 4,*a* shows the distribution of the total specific heat flux q_w over the manikin surface; the flux includes all three components of heat transfer: thermal conductivity, convection, and radiative heat flux. The distribution of the quantity q_{w_rad} reflecting the radiative component of the heat flux is shown in Fig. 4,*b*, and the distribution of the quantity q_{w_conv} including the conductive and convective components is shown in Fig. 4,*c*. These distributions are characterized by strong spatial non-uniformity due to geometry of the manikin and the characteristics of airflow. In particular, the convective heat flux on the front surface of the manikin is significantly higher than on the back surface for incoming flow of cold air.

Table 3 gives the heat fluxes averaged over the elements of the manikin surface (the positions of the elements numbered from I to VI are shown in Fig. 4,*a*; the elements taken for processing the computational data approximately correspond to the experimental setup). The averaging was performed separately for the elements located symmetrically on the left and right sides of the manikin; thus, the total number of elements is 11. Some heat flux asymmetry was observed both in the computations and (to a greater extent) in the experiment. The asymmetry of the computational results can be attributed to some degree of dissymmetry in the geometry and computational mesh.

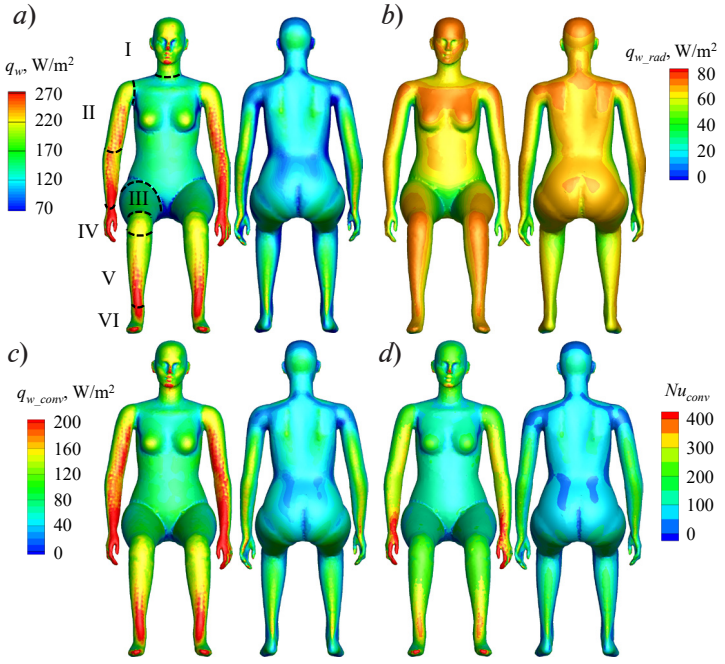

Fig. 4. Distributions of heat fluxes over the manikin surface (Case 1): total (*a*), radiative (*b*), convective (*c*); corresponding distributions of the Nusselt number (*d*); The positions of the elements are numbered from I to VI (see Table 3)

Table 3

Heat fluxes on the surface of the manikin (see Fig. 4)

#	Computed value						Experiment	
	q_w, W/m^2		q_{w_conv}, W/m^2		q_{w_rad}, W/m^2		q_w, W/m^2	
	left	right	left	right	left	right	left	right
I	134.7		68.7		66.0		–	
II	156.0	156.2	98.7	98.9	57.3	57.3	129.6	122.0
III	124.4	123.9	68.2	68.5	56.2	55.4	104.5	100.0
IV	195.8	198.4	145.6	149.5	50.2	48.9	185.2	163.0
V	160.1	160.3	98.3	98.4	61.8	61.9	144.6	142.7
VI	146.0	143.8	88.1	86.7	57.9	58.1	159.7	153.4
∑	139.3		80.5		58.8		122.3	

Notations: q_w, q_{w_conv}, q_{w_rad} are the total, convective and radiative heat fluxes, respectively; the positions on the manikin are numbered from I to VI, ∑ is the sum of fluxes I–VI.

Fig. 4,*d* shows the distribution of dimensionless heat transfer (Nusselt number)

$$\mathrm{Nu}_{conv} = q_{w\_conv} w_m / \lambda (T_w - T_{in}).$$

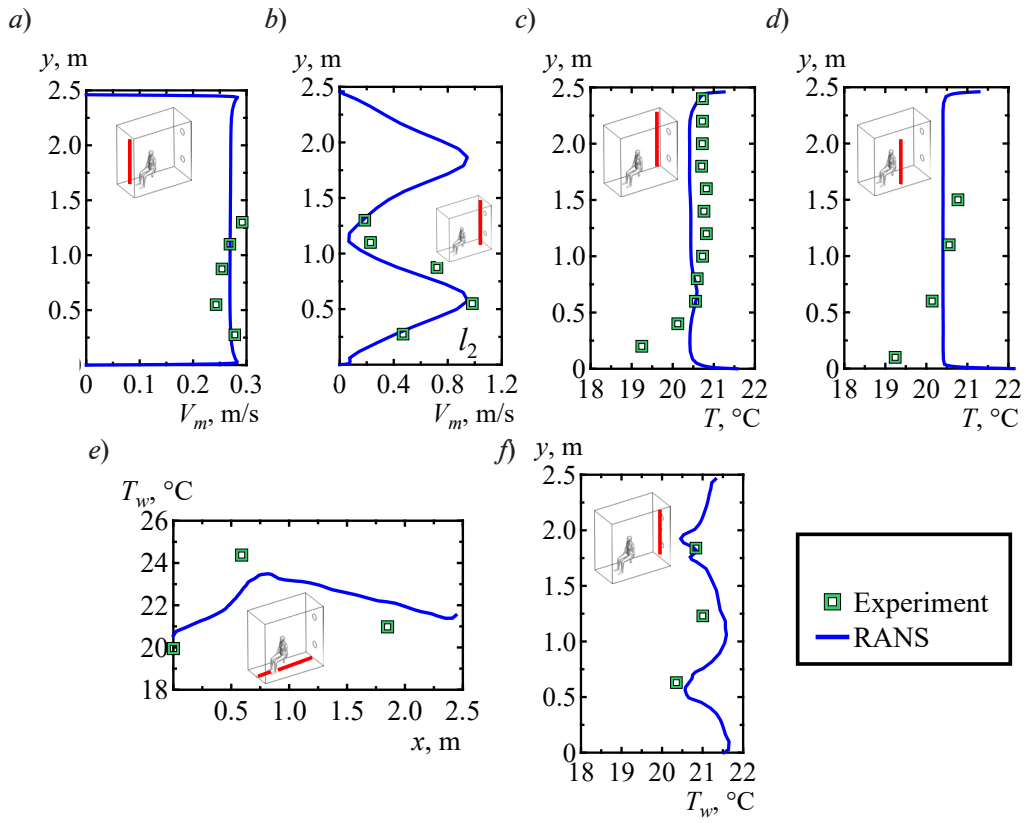

Fig. 5. Computational and experimental velocity profiles in sections l_1 (*a*) and l_2 (*b*); temperature profiles in sections l_3 (*c*) and l_4 (*d*); temperature distribution on the surface of the walls in sections l_5 (*e*) and l_6 (*f*) (see Fig. 1)

We can observe from this distribution that the contribution of the conductive term of heat flux to the total heat transfer is insignificant for the given problem: the Nusselt number averaged over the manikin surface $<Nu_{conv}> = 125$. The local maximum of convective heat transfer is located at the front of the manikin on the hands: the average heat transfer in this region is about 150 W/m^2 (see Table 3), which corresponds to $<Nu_{conv}> = 234$.

Radiative heat flux only slightly varies both over the height of the manikin and locally in its different elements (see Fig. 4,*b* and Table 3), the average value of the radiative term over the manikin surface was 58.8 W/m^2. The total integral heat transfer from the manikin surface is 139.3 W/m^{2}and the integral heat removal from the manikin surface is 223 W. As it turned out for the computational case considered, the contribution from the radiative term of heat flux to the total heat removal was 42%, the contribution from the convective term was 58% (the contribution from the conductive term was less than 1%).

Comparison of computational results with experimental data. We can directly compare the computational results for Case 1 with the experimental data in [30, 31] for the conditions close to experimental ones. Fig. 5, *a*, *b* shows the graphs for the velocity magnitude in the central section of the room, constructed along the vertical lines l_1 and l_2 (see Fig. 1 for the positions of the lines).

The graph in Fig. 5,*a* shows the velocity distribution near the inlet boundary, at a distance of 0.19 m from it. A somewhat non-uniform velocity was detected during the experiment in this section (measurements were carried out only in the lower half of the room). The velocity distribution obtained in the computations based on the boundary condition imposed is almost uniform, with only a small local increase in velocity recorded near the solid walls. The computational and experimental data are generally in good agreement. The velocity distribution shown along the line l_2, located 0.25 m away from the outlet boundary, has two local maxima (the velocity is about 1 m/s), appearing because outlet openings are nearby; the computational and experimental data almost coincide here.

The temperature profiles are shown along two vertical lines: l_3, located in one of the corners of the room near the exits (Fig. 5,*c*), and l_4, located near the manikin (Fig. 5,*d*). The computational temperature profiles are almost uniform, with an increase in the temperature by about 1 degree observed near the walls because they are heated by the radiative heat flux. The experimental data indicate that the temperature profiles are considerably non-uniform, with a pronounced minimum near the floor, while the values at points below 0.5 m turned out to be lower than the inlet temperature $T_{in} = 20.4$ °C, recommended in the documentation for the experimental data and adopted in the computations. The nature of the experimental temperature profiles near the floor may point to some undocumented experimental conditions that cannot be reproduced in computational problems. The computational and experimental temperatures are in good agreement at a height over 0.5 m.

Fig. 5, *e*, *f* compares the computational and experimental data for the surface temperature on the line l_5, passing along the floor, and line l_6, passing along the end wall (crossing the outlet openings). As can be seen from Fig. 5,*e*, a local increase in wall temperature can be observed near the manikin's legs. The local temperature minima in Fig. 5,*f* are due to the presence of the outlet openings. Even though experimental data are scarce, we can conclude from the comparison that the computational and experimental values are in good agreement, including for heating of the walls with external thermal insulation.

The experimental database contains information about the average heat transfer from different elements on the surface of the thermal manikin (see Table 3, two right columns). Documentation does not provide the exact positions for the boundaries of these surfaces, so the experimental data given in Table 3 for the eleven elements only approximately correspond to the processing results of the corresponding computational data. Furthermore, discussing the experimental data presented in [30, 31], the studies do not address the considerable asymmetry of the mean heat flux, with the differences in the values obtained for the left and right elements of the manikin reaching 12%. Nevertheless, qualitative agreement is observed for the spatial inhomogeneities of the heat flux recorded in the computations and in the experiments: the maximum heat transfer in both cases is observed on the hands, and the minimum around the hips. The value of specific heat removal averaged over the entire surface of the manikin obtained computationally was 139.3 W/m^2, exceeding the experimental value of 122.3 W/m^2 by 14%.

Influence of thermal conditions on the manikin surface. One of the reasons for the uncertainty arising in simulations of the human body with a thermal manikin is the type of thermal boundary conditions imposed on the surface. The sensitivity of the flow field and the heat transfer

characteristics to this parameter was estimated in this study based on the computations setting a constant temperature on the surface of the manikin (the conditions corresponding to the experimental setup) and a constant heat flux. In addition, parametric computations were carried for both types of boundary conditions to investigate the radiative contribution to heat transfer.

Case 2 (see Tables 1 and 2) is fully identical with the statement of Case 1, but does not account for the radiative heat transfer. Second-kind boundary conditions were imposed in Cases 3 and 4, the radiative model was activated in Case 3, while radiation was not taken into account in Case 4. Imposing boundary conditions in Case 3, we adopted that q_w = 139.3 W/m², which corresponds to the total heat flux obtained in Case 1, and q_w = 80.5 W/m² in Case 1, which corresponds to the convective term of the heat flux obtained in Case 1. The heat transfer parameters for the four cases are as follows (based on the data in Tables 1 and 2):

Case	Parameter	Mean value over manikin surface
1	q_w, W/m²	139.3
2	q_w, W/m²	80.6
3	T_w, °C	34.2
4	T_w, °C	34.8

Analyzing the computational data, we can conclude that varying the thermal boundary conditions has little effect on the overall structure of the flow: the velocity fields are nearly identical in all four cases (and generally correspond to the illustrations for Case 1 in Figs. 3, *a*, *b* and 5, *a*, *b*). Notably, if the radiative model is deactivated, there is slight rearrangement of the flow in the vicinity of solid boundaries: the mechanism for heating the walls and the near-wall layers of air is switched off in the absence of radiation. Accordingly, the contribution of free convection changes in these layers, and the velocities turn out to be slightly lower.

Fig. 6,*a* shows the distribution of specific convective heat flux over the manikin surface for Case 2. Comparing these data with those in Fig. 4,*c*, we can see that they nearly coincide, which is consistent with the coincidence of the flow structures mentioned above. Evidently, the integral heat removal from the body surface cannot be determined correctly without accounting for radiative heat transfer, since the mean values of the specific total heat flux obtained in Cases 1 and 2 differ significantly.

Temperature distributions obtained in the cases when a constant heat flux (total or convective) was set on the surface are shown in Fig. 6, *b*, *c*. The temperature fields are consistent with the heat flux distributions obtained in the cases with constant surface temperature (compare Fig. 4,*a* with Fig. 6,*b*, and Fig. 6,*a* with 6,*c*). Local heat flux minima correspond to local temperature maxima, and vice versa. We should note that if a heat flux is set at the surface of the manikin, accounting for radiative heat transfer considerably affects the temperature distribution (compare

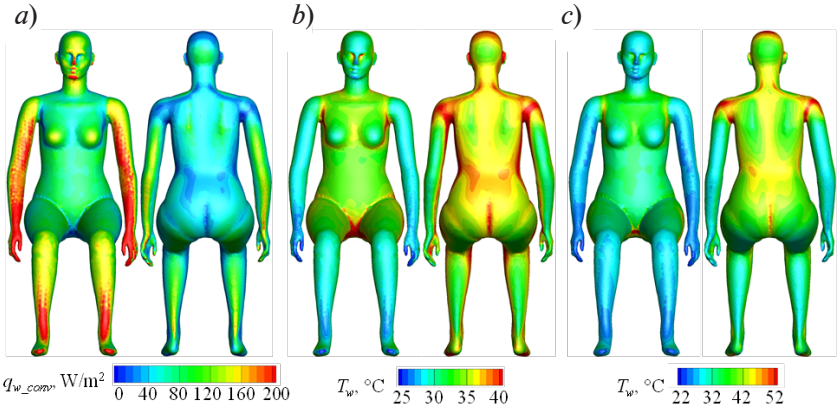

Fig. 6. Distribution of total heat flux over the manikin surface for Case 2 (*a*); distribution of temperature over the manikin surface for Cases 3 (*b*) and 4 (*c*)

Figs. 6,*b* and 6,*c*). A similar spatial structure of the temperature field is observed in both cases, but the temperatures vary in a wider range in the case without accounting for radiative heat transfer, and are higher by 0.6 °C on average.

Characteristics of flow and heat transfer in free-convection flow. The airflow rate set in the experiment provided that forced convection made a significant contribution to determining the flow structure and the heat transfer characteristics. Free-convective heat transfer mechanisms play a major role in problems on ventilation with flow around a heated human body. The contribution from free convection to the evolving processes was analyzed by formulating an additional problem where the inlet air velocity was reduced by 27 times, amounting to V_{in} = 0.01 m/s (see Table 1, Case 5). The statement otherwise coincided with Case 3, where the radiative heat transfer was simulated (see Table 2), and the total heat flux was set on the surface of the manikin.

Fig. 7 shows a comparison of the flow structures and temperature fields for flows with predominantly forced and free convection. As the inlet velocity decreases, the flow structure and, accordingly, the heat transfer characteristics vary significantly. The air in free-convection flow rises slowly along the heated surface of the manikin and moves vertically upward towards the ceiling: a strong thermal plume appears above the manikin. The maximum velocity in this plume reaches 0.34 m/s (see Fig. 7,*e*), which is approximately 40% of the characteristic buoyancy velocity of 0.79 m/s. Buoyant flow impinges on the ceiling and reverses so that regions with recirculation flow appear in front of the manikin and behind it.

Recirculation flow in front of the manikin has a higher intensity because the problem is for-

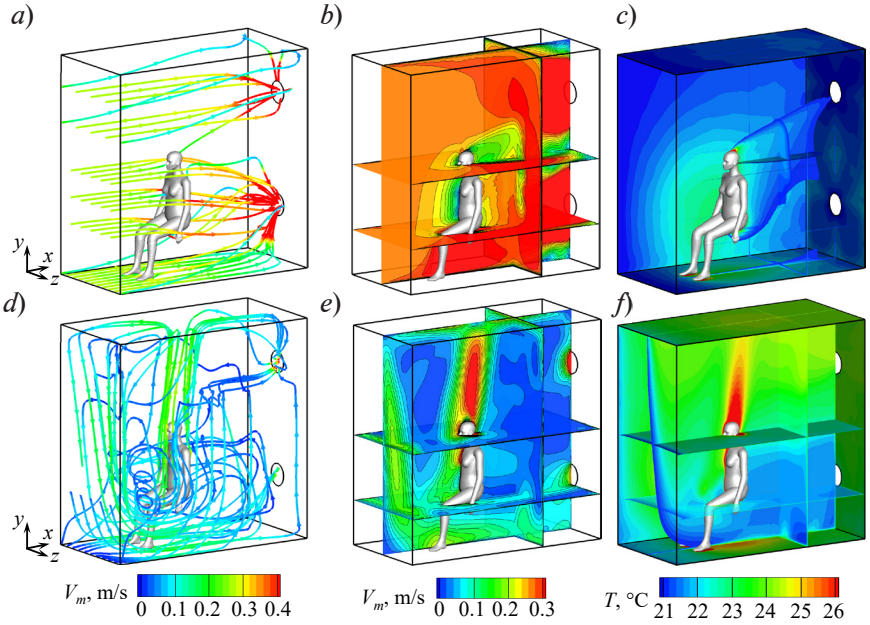

Fig. 7. Structure of airflow in the room for Cases 3 (*a*–*c*) and 5 (*d*–*f*), marked by streamlines colored in accordance with the velocity magnitude (*a*, *d*), as well as the fields of velocity magnitude (*b*, *e*) and temperature (*c, f*) in several sections of the room (*b*, *e*, *f*)

mulated in an asymmetric statement (air flows slowly across the open boundary and is blown out through two opening on the opposite wall): the maximum velocity in the descending jet reaches 0.19 m/s. The flow along the floor is characterized by velocities up to 0.15 m/s, partly drawn into a vertical buoyant jet and partly moving along the floor past the manikin, where it is carried towards the exits.

The free-convection mode is characterized by a stratification of temperature over the height (see Fig. 7, *f*): the flow is heated from the manikin in the upper part of the room, and the temperatures are close to the inlet value in the lower part. Local temperature maxima are observed in the thermal boundary layers near the manikin surface as well as in the thermal plume. In general, the air temperature is higher in Case 5 than in Case 3.

Fig. 8 compares the distributions of temperature and heat flux over the manikin surface for flow with predominantly forced and free convection. As expected, the low intensity of free-convection flow produces a decrease in heat transfer, compared to the flow around the manikin in forced-convection flow (see Fig. 8, *c* and *f*). Accordingly, the surface temperatures of the manikin (Figs. 8, *a* and *d*) increase appreciably (by an average of 4.3 °C): the averaged temperatures over the surface are T_w = 34.2 °C for Case 3 and T_w = 38.5 °C for Case 5. The positions of the local temperature extrema, i.e., the maxima around the torso and forearm, and the minima around the hands and feet, are the same. The increase in surface temperature is accompanied by more intense radiative heat transfer. Provided that the same value of the total heat flux is set in both cases, its components are redistributed: the share of the radiative term was 42.5% in Case 3, the share of the convective term 57.5%, while the shares of radiative and convective terms in Case 5 amounted to 52.5 and 47.5%, respectively (Table 4).

Along with Case 5, two other cases were considered for low flow rate conditions (V_{in} = 0.01 m/s):

Case 6 without accounting for radiation, setting the heat flux equal to the convective component of the heat flux obtained in Case 5 (q_w = 66.1 W/m²) on the surface of the manikin;

Case 7 for weightlessness (the formulation corresponds to Case 5, but the gravitational acceleration is taken to equal zero).

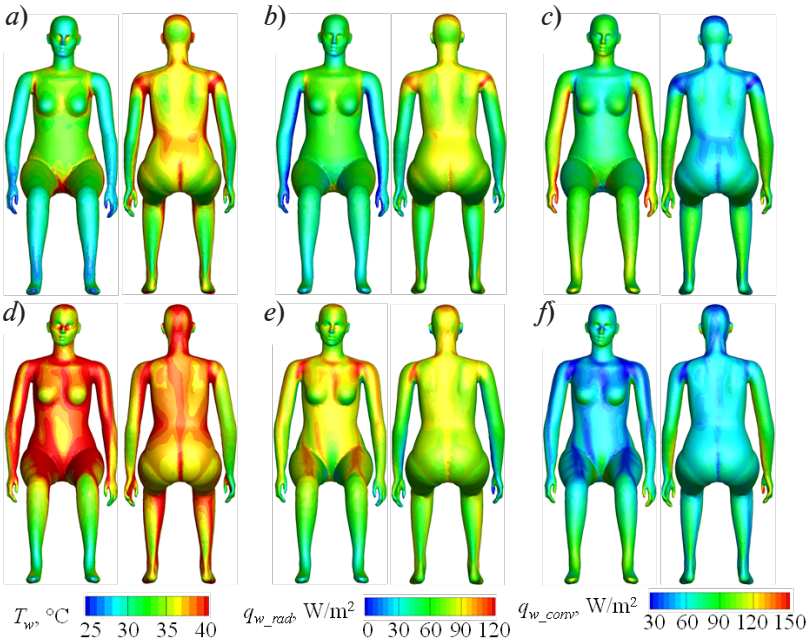

Fig. 8. Fields of temperature (*a, d*), radiative (*b*, *e*) and convective (*c*, *f*) heat fluxes on the surface of the manikin; computational results for cases 3 (*a*–*c*) and 5 (*d* – *f*) are given

Table 4

Parameters of heat transfer from the manikin surface

Case	T_w	q_{w_rad}	q_{w_conv}	q_{w_rad}/q_w	q_{w_conv}/q_w
	°C	W/m²		%	
3	34.2	59.2	80.1	42.5	57.5
5	38.5	73.2	66.1	52.5	47.5
6	38.6	–	66.1	–	100
7	50.2	114.5	24.8	82.2	17.8

The velocity and temperature fields for these cases are shown in Fig. 9 and the temperature distributions over the manikin surface are shown in Fig. 10; the integral heat transfer parameters are summarized in Table 4. Evidently, the results obtained for Case 6 are somewhat different from the data for Case 5: the same as with forced-convection flow (discussed earlier), excluding radiation from analysis does not allow to describe the increase in the wall temperature and the heating of the near-wall regions. In the case of free convection, the absence of heated near-wall layers of air modifies the structure of the flow to a greater extent, decreasing the velocities near the floor; this is accompanied by more intense temperature stratification (see Fig. 9, *c*). The mean temperature over the surface of the manikin is practically the same, about 38.5 °C (see Table 4).

Flow is virtually absent for Case 7 (see Fig. 9, *b*) and the total share of conductive and convective mechanisms of heat transfer was 17.8%. The main contribution to heat transfer is from radiative heat transfer whose share is equal to 82.2%. The walls of the rooms are heated considerably: the temperature averaged over the wall surface was 27.7 °C in Case 7 and 23.8 °C in the baseline Case 5. The surface-averaged temperature of the manikin was 50.2 °C (local values lie in the range from 35.4 to 151.4 °C). Such a high temperature corresponds to a critical value for emergency shutdown of forced ventilation in a spacecraft cabin during an orbital flight (for example, at the International Space Station), without accounting for human thermoregulation mechanisms.

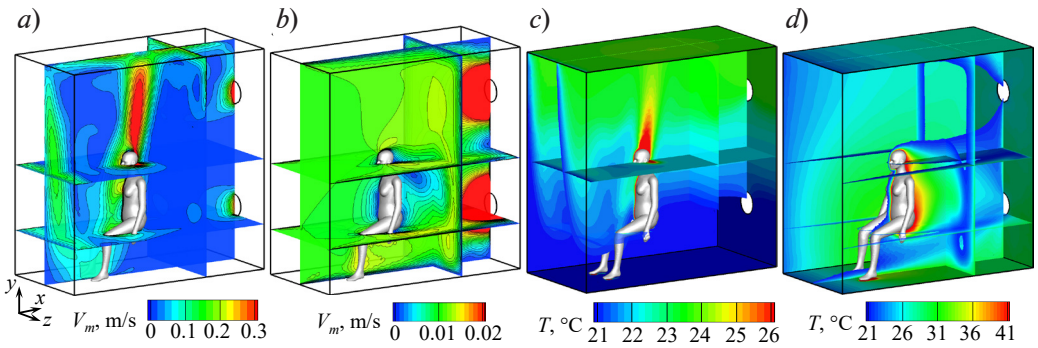

Fig. 9. Fields of velocity magnitude (*a*, *b*) and temperature (*c*, *d*), obtained in computations for Cases 6 (*a*, *c*) and 7 (*b*, *d*) in several sections of the room

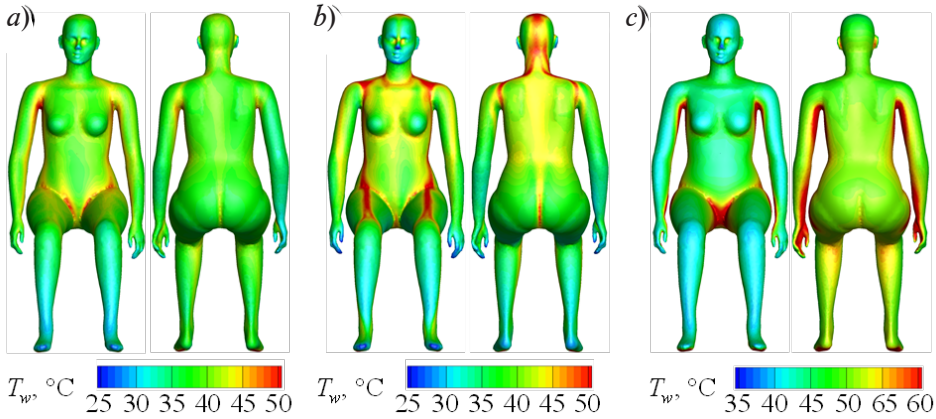

Fig. 10. Temperature distributions over manikin surface obtained in computations for Cases 5 (*a*), 6 (*b*) and 7 (*c*)

Conclusion

The paper presents the results of numerical simulation of three-dimensional turbulent flow and heat transfer in the case of airflow around a seated thermal manikin placed in a model room with mixing ventilation. The computations were carried out in a steady-state formulation based on solving the Reynolds equations closed by the standard k-ε turbulence model; the buoyancy effects were described in the Boussinesq approximation; the radiative energy transfer was taken into account using the Surface-to-surface model. The distributions of velocity and temperature of air in the room, obtained by numerical simulations, are qualitatively and quantitatively consistent with the experimental data presented in the literature. The computational values of specific heat removal from the surface of the manikin were slightly higher than the experimental ones.

Computations were performed in the course of parametric studies both with a constant temperature on the surface of the manikin (which corresponds to the experimental conditions) and with a constant heat flux. We have established that varying the thermal boundary conditions has virtually no effect on the overall structure of the flow, while the general heat release remains consistent. The influence of the radiative contribution to heat transfer was investigated for both types of boundary conditions. It is confirmed that integral heat removal from the surface of a body cannot be determined correctly without accounting for radiative heat transfer: the share of radiative heat flux exceeded 40%. In addition, accounting for radiation affects the computed temperature of room walls and the airflow in the near-wall layers.

Along with studies of ventilation with predominantly forced convection (corresponding to the experiment), we also considered the characteristics of flow and heat transfer for free convection. We have observed that the structure of the flow under predominantly free convection is determined by a strong thermal plume evolving above the manikin and the temperature field is stratified by height. The free-convection conditions with low-velocity airflow is characterized by lower values of heat transfer compared to the flow around a manikin under forced convection, which is accompanied by an increase in the surface temperature and more intense radiative heat transfer.

REFERENCES

1. **Grimitlin M. I.,** Raspredelenie vozdukha v pomeshcheniyakh [Air distribution in the rooms], 3rd Ed., AVOK Severo-Zapad, St. Petersburg, 2004 (in Russian).

2. **Awbi H. S.,** Ventilation of buildings, Taylor & Francis Group (Spon Press), London, 2005.

3. **Hurnik M., Blaszczok M., Popiolek Z.,** Air distribution measurement in a room with a sidewall jet: A 3D benchmark test for CFD validation, Build. Environ. 2015. Vol. 93-2 (November) (2015) 319–330.

4. **Markov D., Ivanov N., Pichurov G., et al.,** On the procedure of draught rate assessment in indoor spaces, Appl. Sci. 10 (15) (2020) 5036.

5. **Yamasawa H., Kobayashi T., Yamanaka T., et al.,** Experimental investigation of difference in indoor environment using impinging jet ventilation and displacement ventilation systems, Int. J. Vent., Publ, 27 Jan. 2021 (18 p.) https://doi.org/10.1080/ 14733315. 2020. 1864572.

6. **Nilsson H. O., Comfort** climate evaluation with thermal manikin methods and computer simulation models. Ph. D thesis, Royal Inst. Technol., Depart. of Civil and Architect. Eng., Sweden, 2004.

7. **Kilic M., Sevilgen G.,** Evaluation of heat transfer characteristics in an automobile cabin with a virtual manikin during heating period, Numer. Heat Transf. A. 56 (6) (2009) 515–539.

8. **Yang C., Zhang X., Yao Z., He F.,** The Large Eddy Simulation and stability analysis of flow field in a generic cabin, Proc. Eng. 121 (2015) 1749–1756.

9. **Croitoru C., Nastase I., Bode F., Cojocaru G.,** Assessment of virtual thermal manikins for thermal comfort numerical studies. Verification and validation, E3S Web Conf. 111 (CLIMA 2019 Congress) (2019) 02018.

10. **Kabanshi A., Wigö H., Sandberg M.,** Experimental evaluation of an intermittent air supply system. P. 1: Thermal comfort and ventilation efficiency measurements, Build. Environ. 95 (January) (2016) 240–250.

11. **Villi G., De Carli M.,** Detailing the effects of geometry approximation and grid simplification on the capability of a CFD model to address the benchmark test case for flow around a computer simulated person, Build. Simul. 7 (1) (2014) 35–55.

12. **Zukowska D., Melikov A., Popiolek Z.,** Thermal plume above a simulated sitting person with different complexity of body geometry, Proc. Roomvent 2007 (Conf. at Helsinki, 13–15 June, 2007). 3 (2007) 191–198.

13. **Yan Y., Li X., Yang L., Tu J.,** Evaluation of manikin simplification methods for CFD simulations in occupied indoor environments, Energy Build. 127 (1 September) (2016) 611–626.

14. **Stepasheva E. D., Zasimova M. A., Ivanov N. G.,** Thermal manikin shape influence on airflow and heat transfer in the model room with displacement ventilation, St. Petersburg State Polytechnical University Journal. Physics and Mathematics. 14 (3) (2021) 90–106.

15. **Saarinen P. E., Kalliomäki P., Tang J. W., Koskela H.,** Large Eddy Simulation of air escape through a hospital isolation room single hinged doorway – validation by using tracer gases and simulated smoke videos, PLoS ONE. 10 (7) (2015) e0130667.

16. **Feng L., Zeng F., Li R., Ju R., Gao N.,** Influence of manikin movement on temperature stratification in a displacement ventilated room, Energy Build. 234 (1 March) (2021) 110700.

17. **Oguro M., Arens E., de Dear R.J., et al.,** Convective heat transfer coefficients and clothing insulations for parts of the clothed human body under airflow conditions, J. Archit. Plan. (Trans. AIJ). 67 (561) (2002) 21–29.

18. **Oliveira A. V. M., Branco V. J., Gaspar A. R., Quintela D. A.,** Measuring thermal insulation of clothing with different manikin control methods. Comparative analysis of the calculation methods, Proc. 7th Int. Thermal Manikin and Model. Meeting (at Univ. of Coimbra, Portugal), September, 2008.

19. **Wang C., Yoo S.-J., Tanabe S., Ito K.,** Investigation of transient and heterogeneous microclimate around a human body in an enclosed personalized work environment, Energy Built Environ. 1 (4) (2020) 423–431.

20. **Ivanov M., Mijorski S.,** CFD modelling of flow interaction in the breathing zone of a virtual thermal manikin, Energy Proc. 112 (March) (2017) 240–251.

21. **Gao N. P., Niu J. L.,** CFD Study of the thermal environment around a human body: A review, Indoor Built Environ. 14 (1) (2005) 5–16.

22. **Yan Y., Li X., Tu J.,** Thermal effect of human body on cough droplets evaporation and dispersion in an enclosed space, Build. Environ. 148 (15 January) (2019) 96–106.

23. **Gao N., Niu J., Morawska L.,** Distribution of respiratory droplets in enclosed environments under different air distribution methods, Build. Simul. 1 (4) (2008) 326–335.

24. **Xu C., Wei X., Liu L., et al.,** Effects of personalized ventilation interventions on airborne infection risk and transmission between occupants, Build. Environ. 180 (August) (2020) 107008.

25. **Van Hooff T., Blocken B., Tominaga Y.,** On the accuracy of CFD simulations of cross-ventilation flows for a generic isolated building: comparison of RANS, LES and experiments, Build. Environ. 114 (March) (2017) 148–165.

26. **Zasimova M. A., Ivanov N. G., Markov D.,** Numerical modeling of air distribution in a test room with 2D sidewall jet. I. Foundations for eddy resolving approach application based on periodical formulation, St. Petersburg State Polytechnical University Journal. Physics and Mathematics. 13 (3) (2020) 56–74.

27. **Zasimova M. A., Ivanov N. G., Markov D.,** Numerical modeling of air distribution in a test room with 2D sidewall jet. II. LES-computations for the room with finite width, St. Petersburg State Polytechnical University Journal. Physics and Mathematics. 13 (3) (2020) 75–92.

28. **Nielsen P. V., Murakami S., Kato S., et al.,** Benchmark tests for a computer simulated person, Indoor Environmental Engineering, Aalborg University, Denmark, 2003.

29. **Topp C., Hesselholt P., Trier M. R., Nielsen P. V.,** Influence of geometry of thermal manikins on room airflow, Proc. ISIAQ 7th Int. Conf. "Healthy Buildings 2003", Singapore, December 7–22, 2003.

30. **Nilsson H., Brohus H., Nielsen P.,** Benchmark test for a computer simulated person – manikin heat loss for thermal comfort evaluation, Indoor Environmental Engineering, Aalborg University, Denmark, 2007.

31. **Nilsson H., Brohus H., Nielsen P.,** CFD modeling of thermal manikin heat loss in a comfort evaluation benchmark test, Proc. Roomvent 2007 (Conf. at Helsinki, 13–15 June, 2007), 2007.

32. **Taghinia J. H., Rahman M. M., Lu X.,** Effects of different CFD modeling approaches and simplification of shape on prediction of flow field around manikin, Energy Build. 170 (1 July) (2018) 47–60.

33. **Deevy M., Sinai Y., Everitt P., et al.,** Modelling the effect of an occupant on displacement ventilation with computational fluid dynamics, Energy Build. 40 (3) (2008) 255–264.

34. **Martinho N., Lopes A., Silva M.,** CFD modelling of benchmark tests for flow around a detailed computer simulated person, Proc. 7th Int. Thermal Manikin and Model. Meeting (at Univ. of Coimbra, Portugal). September, 2008.

35. **Martinho N., Lopes A., da Silva M. G.,** Evaluation of errors on the CFD computation of air flow and heat transfer around the human body, Build. Environ. 58 (December) (2012) 58–69.

36. **Siodlaczek M., Gaedtke M., Simonis S., et al.,** Numerical evaluation of thermal comfort using a large eddy lattice Boltzmann method, Build. Environ. 192 (April) (2021) 107618.

37. **Smirnov E. M., Ivanov N. G., Telnov D. S., Son C. H.,** CFD modeling of cabin air ventilation in the International Space Station: A comparison of RANS and LES data with test measurements for the Columbus Module, Int. J. Vent. 5 (2) (2006) 219–228.

38. **Ivanov N. G., Telnov D. S., Smirnov E. M., Son C. H.,** Propagation of CO_2 field after fire extinguisher discharge: A numerical study, Proc. 41st Int. Conf. Environ. Syst. (AIAA); Portland, Oregon, July 2011. Rep. AIAA 2011-5078.

39. **Wilcox D. C.,** Turbulence modeling for CFD, 3-th Ed., DCW Industries, Inc., California, La Cacada, 2006.

СПИСОК ЛИТЕРАТУРЫ

1. **Гримитлин М. И.** Распределение воздуха в помещениях. СПб.: Изд-во «АВОК Северо-Запад», 2004. 320 с.

2. Awbi H. S. Ventilation of buildings. London: Taylor & Francis Group (Spon Press), 2005. 522 p.

3. **Hurnik M., Blaszczok M., Popiolek Z.** Air distribution measurement in a room with a sidewall jet: a 3D benchmark test for CFD validation // Building and Environment. 2015. Vol. 93. Part 2. November. Pp. 319–330.

4. **Markov D., Ivanov N., Pichurov G., Zasimova M., Stankov P., Smirnov E., Simova I., Ris V., Angelova R., Velichkova R.** On the procedure of draught rate assessment in indoor spaces // Applied Sciences. 2020. Vol. 10. No. 15. P. 5036.

5. **Yamasawa H., Kobayashi T., Yamanaka T., Choi N, Matsuzaki M.** Experimental investigation of difference in indoor environment using impinging jet ventilation and displacement ventilation systems // International Journal of Ventilation. Published 27 Jan. 2021 (18 p.) https://doi.org/10.1080/14733315. 2020. 1864572.

6. **Nilsson H. O.** Comfort climate evaluation with thermal manikin methods and computer simulation models. Ph. D thesis. Royal Institute of Technology. Department of Civil and Architectural Engineering. Sweden, 2004. 202 p.

7. **Kilic M., Sevilgen G.** Evaluation of heat transfer characteristics in an automobile cabin with a virtual manikin during heating period // Numerical Heat Transfer. Part A. 2009. Vol. 56. No. 6. Pp. 515–539.

8. **Yang C., Zhang X., Yao Z., He F.** The Large Eddy Simulation and stability analysis of flow field in a generic cabin // Procedia Engineering. 2015. Vol. 121. Pp. 1749–1756.

9. **Croitoru C., Nastase I., Bode F., Cojocaru G.** Assessment of virtual thermal manikins for thermal comfort numerical studies. Verification and validation // E3S Web of Conferences. 2019. Vol. 111. CLIMA 2019 Congress. P. 02018.

10. **Kabanshi A., Wigö H., Sandberg M.** Experimental evaluation of an intermittent air supply system e Part 1: Thermal comfort and ventilation efficiency measurements // Building and Environment. 2016. Vol. 95. January. Pp. 240–250.

11. **Villi G., De Carli M.** Detailing the effects of geometry approximation and grid simplification on the capability of a CFD model to address the benchmark test case for flow around a computer simulated person // Building Simulation. 2014. Vol. 7. No. 1. Pp. 35–55.

12. **Zukowska D., Melikov A., Popiolek Z.** Thermal plume above a simulated sitting person with different complexity of body geometry // Proceedings of Roomvent 2007 (Conference at Helsinki, 13–15 June, 2007). Finland, 2007. Vol. 3. Pp. 191–198.

13. **Yan Y., Li X., Yang L., Tu J.** Evaluation of manikin simplification methods for CFD simulations in occupied indoor environments // Energy and Buildings. 2016. Vol. 127. 1 September. Pp. 611–626.

14. **Степашева Е. Д., Засимова М. А., Иванов Н. Г.** Влияние формы теплового манекена на течение и теплообмен в модельном помещении с вытесняющей вентиляцией // Научно-технические ведомости СПбГПУ. Физико-математические науки. 2021. Т. 14. № 3. С. 94–111.

15. **Saarinen P. E., Kalliomäki P., Tang J. W., Koskela H.** Large Eddy Simulation of air escape through a hospital isolation room single hinged doorway – validation by using tracer gases and simulated smoke videos // PLoS ONE. 2015. Vol. 10. No. 7. P. e0130667.

16. **Feng L., Zeng F., Li R., Ju R., Gao N.** Influence of manikin movement on temperature stratification in a displacement ventilated room // Energy and Buildings. 2021. Vol. 234. 1 March. P. 110700.

17. **Oguro M., Arens E., de Dear R.J., Zhang H., Katayama,** T. Convective heat transfer coefficients and clothing insulations for parts of the clothed human body under airflow conditions // Journal of Architecture and Planning (Transactions of AIJ). 2002. Vol. 67. No. 561. Pp. 21–29.

18. **Oliveira A. V. M., Branco V. J., Gaspar A. R., Quintela D. A.** Measuring thermal insulation of clothing with different manikin control methods. Comparative analysis of the calculation methods // Proceedings of the 7th International Thermal Manikin and Modelling Meeting (at University of Coimbra, Portugal). September, 2008. 7 p.

19. **Wang C., Yoo S.-J., Tanabe S., Ito K.** Investigation of transient and heterogeneous microclimate around a human body in an enclosed personalized work environment // Energy and Built Environment. 2020. Vol. 1. No. 4. Pp. 423–431.

20. **Ivanov M., Mijorski S.** CFD modelling of flow interaction in the breathing zone of a virtual thermal manikin // Energy Procedia. 2017. Vol. 112. March. Pp. 240–251.

21. **Gao N. P., Niu J. L.** CFD Study of the thermal environment around a human body: A review // Indoor and Built Environment. 2005. Vol. 14. No. 1. Pp. 5–16.

22. **Yan Y., Li X., Tu J.** Thermal effect of human body on cough droplets evaporation and dispersion in an enclosed space // Building and Environment. 2019. Vol. 148. 15 January. Pp. 96–106.

23. **Gao N., Niu J., Morawska L.** Distribution of respiratory droplets in enclosed environments under different air distribution methods // Building Simulation. 2008. Vol. 1. No. 4. Pp. 326–335.

24. **Xu C., Wei X., Liu L., Su L., Liu W., Wang Y., Nielsen P. V.** Effects of personalized ventilation interventions on airborne infection risk and transmission between occupants // Building and Environment. 2020. Vol. 180. August. P. 107008.

25. **Van Hooff T., Blocken B., Tominaga Y.** On the accuracy of CFD simulations of cross-ventilation flows for a generic isolated building: comparison of RANS, LES and experiments // Building and Environment. 2017. Vol. 114. March. Pp. 148–165.

26. **Засимова М. А., Иванов Н. Г., Марков Д.** Численное моделирование циркуляции воздуха в помещении при подаче из плоской щели. Часть 1: отработка применения вихреразрешающего подхода с использованием периодической постановки // Научно-технические ведомости СПбГПУ. Физико-математические науки. 2020. Т. 13. № 3. С. 56–74.

27. **Засимова М. А., Иванов Н. Г., Марков Д.** Численное моделирование циркуляции воздуха в помещении при подаче из плоской щели. Часть 2: LES-расчеты для помещения конечной ширины // Научно-технические ведомости СПбГПУ. Физико-математические науки. 2020. Т. 13. № 3. С. 75–92.

28. **Nielsen P. V., Murakami S., Kato S., Topp C., Yang J.-H.** Benchmark tests for a computer simulated person. Aalborg University, Denmark: Indoor Environmental Engineering, 2003. October. 7 p. ISSN 1395-7953 R0307.

29. **Topp C., Hesselholt P., Trier M. R., Nielsen P. V.** Influence of geometry of thermal manikins on room airflow // Proceedings of ISIAQ 7th International Conference "Healthy Buildings 2003". Singapore, December 7–22, 2003. 6 p.

30. **Nilsson H., Brohus H., Nielsen P.** Benchmark test for a computer simulated person – manikin heat loss for thermal comfort evaluation. Aalborg University, Denmark: Indoor Environmental Engineering, Aalborg University, 2007. 7 p.

31. **Nilsson H., Brohus H., Nielsen P.** CFD modeling of thermal manikin heat loss in a comfort evaluation benchmark test // Proceedings of Roomvent 2007 (Conference at Helsinki, 13 – 15 June, 2007). Finland, 2007. (7 p.)

32. **Taghinia J. H., Rahman M. M., Lu X.** Effects of different CFD modeling approaches and simplification of shape on prediction of flow field around manikin // Energy and Buildings. 2018. Vol. 170. 1 July. Pp. 47–60.

33. **Deevy M., Sinai Y., Everitt P., Voigt L., Gobeau N.** Modelling the effect of an occupant on displacement ventilation with computational fluid dynamics // Energy and Buildings. 2008. Vol. 40. No. 3. Pp. 255–264.

34. **Martinho N., Lopes A., Silva M.** CFD modelling of benchmark tests for flow around a detailed computer simulated person // Proceedings of the 7th International Thermal Manikin and Modelling Meeting (at University of Coimbra, Portugal). September, 2008. 6 p.

35. **Martinho N., Lopes A., da Silva M. G.** Evaluation of errors on the CFD computation of air flow and heat transfer around the human body // Building and Environment. 2012. Vol. 58. December. Pp. 58–69.

36. **Siodlaczek M., Gaedtke M., Simonis S., Schweiker M., Homma N., Krause M. J.** Numerical evaluation of thermal comfort using a large eddy lattice Boltzmann method // Building and Environment. 2021. Vol. 192. April. P. 107618.

37. **Smirnov E. M., Ivanov N. G., Telnov D. S., Son C. H.** CFD modeling of cabin air ventilation in the International Space Station: a comparison of RANS and LES data with test measurements for the Columbus Module // International Journal of Ventilation. 2006. Vol. 5. No. 2. Pp. 219–228.

38. **Ivanov N. G., Telnov D. S., Smirnov E. M., Son C. H.** Propagation of CO_2 field after fire extinguisher discharge: A numerical study // Proceedings of the 41st International Conference on Environmental Systems. American Institute of Aeronautics and Astronautics (AIAA); Portland, Oregon, July 2011. Report No. AIAA 2011-5078 (8 p.).

39. **Wilcox D. C.** Turbulence modeling for CFD. 3-th Ed. La Cacada, California: DCW Industries, Inc., 2006. 515 p.

THE AUTHORS

ZASIMOVA Marina A.
Peter the Great St. Petersburg Polytechnic University
29 Politechnicheskaya St., St. Petersburg, 195251, Russia
zasimova_ma@spbstu.ru
ORCID: 0000-0002-4103-6574

MARINOVA Alexandra A.
Peter the Great St. Petersburg Polytechnic University
29 Politechnicheskaya St., St. Petersburg, 195251, Russia
sanmarinova@gmail.com
ORCID: 0000-0002-9612-5814

IVANOV Nikolay G.
Peter the Great St. Petersburg Polytechnic University
29 Politechnicheskaya St., St. Petersburg, 195251, Russia
ivanov_ng@spbstu.ru
ORCID: 0000-0001-9897-5401

PODMARKOVA Anna D.
Peter the Great St. Petersburg Polytechnic University
29 Politechnicheskaya St., St. Petersburg, 195251, Russia
ann.podmarkova@mail.ru
ORCID: 0000-0002-8329-7094

СВЕДЕНИЯ ОБ АВТОРАХ

ЗАСИМОВА Марина Александровна – *кандидат физико-математических наук, доцент Высшей школы прикладной математики и вычислительной физики Санкт-Петербургского политехнического университета Петра Великого.*
195251, Россия, г. Санкт-Петербург, Политехническая ул., 29
zasimova_ma@spbstu.ru
ORCID: 0000-0002-4103-6574

МАРИНОВА Александра Андреевна – *студентка Высшей школы прикладной математики и вычислительной физики Санкт-Петербургского политехнического университета Петра Великого.*
195251, Россия, г. Санкт-Петербург, Политехническая ул., 29
sanmarinova@gmail.com
ORCID: 0000-0002-9612-5814

ИВАНОВ Николай Георгиевич – *кандидат физико-математических наук, доцент Высшей школы прикладной математики и вычислительной физики, заведующий научно-исследовательской лабораторией гидроаэродинамики Санкт-Петербургского политехнического университета Петра Великого.*
195251, Россия, г. Санкт-Петербург, Политехническая ул., 29
ivanov_ng@spbstu.ru
ORCID: 0000-0001-9897-5401

ПОДМАРКОВА Анна Дмитриевна – *аспирантка Высшей школы прикладной математики и вычислительной физики Санкт-Петербургского политехнического университета Петра Великого.*
195251, Россия, г. Санкт-Петербург, Политехническая ул., 29
ann.podmarkova@mail.ru
ORCID: 0000-0002-8329-7094

Received 16.06.2022. Approved after reviewing 28.06.2022. Accepted 28.06.2022.
Статья поступила в редакцию 16.06.2022. Одобрена после рецензирования 28.06.2022. Принята 28.06.2022.